Ultrasonics 54 (2014) 1186–1196

Contents lists available at ScienceDirect

Ultrasonics

journal homepage: www.elsevier.com/locate/ultras

On ultrasound waves guided by bones with coupled soft tissues: A mechanism study and *in vitro* calibration

Jiangang Chen, Zhongqing Su *

The Department of Mechanical Engineering, The Hong Kong Polytechnic University, Kowloon, Hong Kong

ARTICLE INFO

Article history:
Available online 17 August 2013

Keywords:
Bone assessment
Coupling effect
Quantitative ultrasound (QUS)
Soft tissue
Ultrasound waves

ABSTRACT

The influence of soft tissues coupled with cortical bones on precision of quantitative ultrasound (QUS) has been an issue in the clinical bone assessment in conjunction with the use of ultrasound. In this study, the effect arising from soft tissues on propagation characteristics of guided ultrasound waves in bones was investigated using tubular Sawbones phantoms covered with a layer of mimicked soft tissue of different thicknesses and elastic moduli, and an *in vitro* porcine femur in terms of the axial transmission measurement. Results revealed that presence of soft tissues can exert significant influence on the propagation of ultrasound waves in bones, leading to reduced propagation velocities and attenuated wave magnitudes compared with the counterparts in a free bone in the absence of soft tissues. However such an effect is not phenomenally dependent on the variations in thickness and elastic modulus of the coupled soft tissues, making it possible to compensate for the coupling effect regardless of the difference in properties of the soft tissues. Based on an *in vitro* calibration, this study proposed quantitative compensation for the effect of soft tissues on ultrasound waves in bones, facilitating development of high-precision QUS.

1. Introduction

The increasing needs for monitoring the bone health status, for example diagnosis of osteoporosis, have entailed a number of quantitative bone assessment techniques, typified by quantitative ultrasound (QUS), X-ray computed tomography (CT) and magnetic resonant imaging (MRI) [1–3]. In particular, QUS has been deemed as a most promising candidate for quantitative bone evaluation, due to its competitive nature of non-radiation, ease of manipulation and cost-effectiveness [1]. With the application of various measurement configurations, the ultrasonic waves can be injected into the bone structure and captured after they propagate either axially along the bone axis (i.e., axial transmission (AT)), or circumferentially across the bone cross-section (i.e., transverse transmission), or in the bone thickness in a reflection manner (i.e., pulse echo or backscattering) [1,4–12]. The bone properties can be evaluated in different respects with applications of different techniques, among which the AT technique remains most competitive, because it is capable to reflect not only the material properties of the bone, but the bone geometrical features [13–16]. With such a fascination, the AT-based QUS has gained a good reputation as promising for osteoporosis evaluation [15–18].

However, the prevalence of such a technique has been considerably undermined by the fact that the soft tissue covering the bone introduces unwanted disturbances and severe alterations to the propagation of ultrasonic waves in the bone, significantly preventing the AT-based QUS technique toward a clinical application of high precision and accuracy [17,19–25]. With such a concern, considerable efforts have been directed to developing novel methods to remove the influence of soft tissues. In this regard, Moilanen et al. [26] invented an axial transmission device with receiver shifted at a constant step during the measurement. With such an operation, a distance–time diagram was obtained, from which the wave propagation velocities can be determined without the interference from the overlying soft tissues. Bossy et al. [17] developed a bidirectional transmission technique using a probe consisting of two groups of emitters with a single group of receivers in between. The generated ultrasound waves travel along the bone in opposite directions. By taking into account time delays of waves propagating in opposite directions, influence arising from unequal thicknesses of the coupled soft tissues and the probe inclination can be compensated for. However, previous efforts considered the soft tissue as an addition layer to the bone that only provide extra wave propagation routines. The coupling effect on wave propagation in real bone structures has not been explored but is of great importance.

Our previous results demonstrated that a coupling layer (fluid or mimicked soft tissue) can significantly alter the wave

* Corresponding author. Tel.: +852 2766 7818; fax: +852 2365 4703.
E-mail address: MMSU@polyu.edu.hk (Z. Su).

0041-624X/$ - see front matter © 2013 Elsevier B.V. All rights reserved.
http://dx.doi.org/10.1016/j.ultras.2013.08.002

propagation characteristics in solid wave guides (i.e., metal or bone-mimicking plate) [19–21,27,28]. However, the coupling effect on wave propagation in real bone structures which is much different from plates has not been explored but of great significance. With such a concern, in this study, a series of tubular Sawbones samples covered with a layer of artificial silicon rubber (ASR) (serving as mimicked soft tissue and considered as *Tissue Equivalent Materials* (TEM)) varied in thickness and elastic modulus was ultrasonically interrogated at multiple frequencies, as well as an *in vitro* porcine femur with soft tissue but marrow removed. The propagation characteristics of the first arrival signal (FAS) and second arrival signal (SAS) in the soft tissue–bone mimicking phantoms and *in vitro* porcine femur were analyzed. This study further contributes to the understanding of the soft tissue coupling effect on the propagation of ultrasonic guided waves, paving the way for development of high-precision QUS techniques for clinical bone assessment.

2. Ultrasound waves in a coupled cylindrical medium

Ultrasonic wave propagation in soft tissue–bone-coupled (SBC) media can be simplified to wave propagation in a fluid–solid bilayer (FSB) for a first level approximation, by regarding the soft tissue as fluid [17,23,26,29]. Here, the analytical description of wave propagation in the coupled media, in particular in the tubular structure, is recalled, treating the bone as a sort of tubular structure.

First, considering a homogeneous, isotropic and elastic medium, the equation of particulate motion in the medium can be expressed as [30]

$$\mu\nabla^2 u + (\lambda+\mu)\nabla(\nabla\cdot u) = \rho\frac{\partial^2 u}{\partial t^2}, \tag{1}$$

where u, ρ, λ and μ are the displacement field, density and the two Lamé constants of the material, respectively. In a FSB as illustrated in Fig. 1, the displacement (u) in either the solid or fluid part can be decomposed as, according to the Helmholtz decomposition [31],

$$u = -\nabla\Phi + \nabla\times\Psi, \tag{2}$$

where Φ is the scalar potential, and Ψ the vector potential. Therein, the displacement in a solid cylinder can be decomposed by its corresponding scalar potential (Φ^S) and vector potential (Ψ^S) as [23]

$$\Phi^S = [A_1 J_n(\alpha r) + A_2 Y_n(\alpha r)]\cdot\cos(n\theta)\cdot e^{i(k_z z-\omega t)}, \tag{3a}$$

$$\Psi_r^S = [B_1 J_{n+1}(\beta r) + B_2 Y_{n+1}(\beta r)]\cdot\cos(n\theta)\cdot e^{i(k_z z-\omega t)}, \tag{3b}$$

$$\Psi_\theta^S = -[B_1 J_{n+1}(\beta r) + B_2 Y_{n+1}(\beta r)]\cdot\cos(n\theta)\cdot e^{i(k_z z-\omega t)}, \tag{3c}$$

$$\Psi_z^S = [C_1 J_{n+1}(\beta r) C_2 Y_{n+1}(\beta r)]\cdot\sin(n\theta)\cdot e^{i(k_z z-\omega t)}, \tag{3d}$$

As fluid is unable to sustain shear stresses, the vector potential of displacement in fluid remains zero. As a result, the displacement in fluid can only be express by the scalar potential, namely [19]

$$\Phi^F = [D_1 J_n(\alpha^F r) + D_2 Y_n(\alpha^F r)]\cdot\cos(n\theta)\cdot e^{i(k_z z-\omega t)} \tag{4}$$

In Eqs. (3) and (4), $\alpha^2 = \omega^2/C_L^2 - k^2$, $\beta^2 = \omega^2/C_T^2 - k^2$, $\alpha^{F^2} = \omega^2/C_F^2 - k^2$. J_n and Y_n are Bessel functions of the order n. ω, k, C_L, C_T, C_F are the angular frequency, wavenumber, longitudinal wave velocity in solid, transverse wave velocity in solid and longitudinal wave velocity in fluid, respectively. Note that k_Z is the wavenumber in dimension Z, while k is the wavenumber of dimensionless.

At the interface of the fluid and solid, only normal components of the displacement and stress are continuous, while the continuity of the shear components never holds. The boundary conditions are [32]

$$\begin{aligned} &\sigma_{rr} = \sigma_{r\theta} = \sigma_{rz} = 0, \quad \text{at } r = a \\ &u_r = u_r^F,\ \sigma_{rr} = \sigma_{rr}^F,\ \sigma_{r\theta} = \sigma_{rz} = 0, \quad \text{at } r = a + h_s \\ &\sigma_r^F = 0 \quad \text{at } r = a + h_s + h_F \end{aligned} \tag{5}$$

where σ_{rr}, $\sigma_{r\theta}$, σ_{rz} are the three stress components in the cylindrical coordinate. u_r, σ_{rr} and $\sigma_{r\theta}$ are the radial (or normal) component of displacement and stress, circumferential component of stress in the solid, respectively. u_r^F, σ_r^F and σ_{rz} are the radial (or normal) component of displacement and stress, circumferential component of stress in the fluid, respectively. a, h_S and h_F are the inner radius, thickness of the solid cylinder and thickness of the fluid layer, respectively, as indicated in Fig. 1. Combining the boundary conditions (i.e., Eq. (5)) together with the governing wave equations (i.e., Eqs. (3) and (4)), it yields the characteristic equation of ultrasonic wave propagating in the FSB, i.e., the determinant of the coefficient matrix consisting of $A_1, A_2, \ldots, D_2$ in Eqs. (3) and (4), (more details can be referred to elsewhere [19])

$$|M = 0|. \tag{6}$$

Based on Eq. (6), Fig. 2 plots the dispersion curves of cylindrical Lamb waves in a cortical bone cylinder (inner radius: 4 mm; wall thickness: 3 mm; material properties are shown in Table 1) in the absence and presence of a layer of fluid (thickness: 1 mm, as listed Table 1), to find that the features of the guided modes in the bone cylinder coated with a layer of fluid behave much

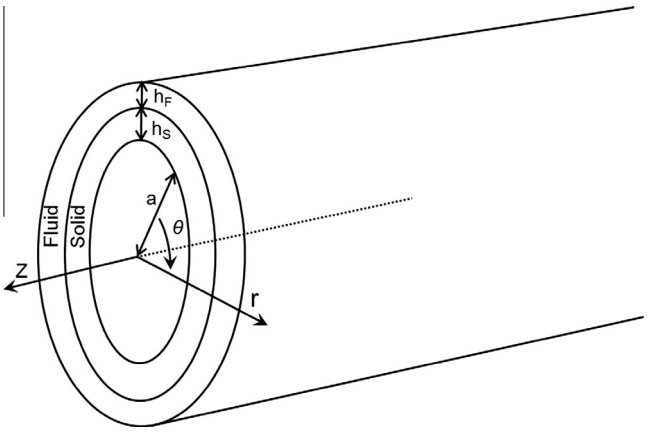

Fig. 1. A hollow cylinder covered with a layer of fluid of an infinite extent in z-direction and a finite thickness in the cylindrical coordinates (a: inner radius of the cylinder, h_S: thickness of the cylinder, h_F: thickness of the fluid layer).

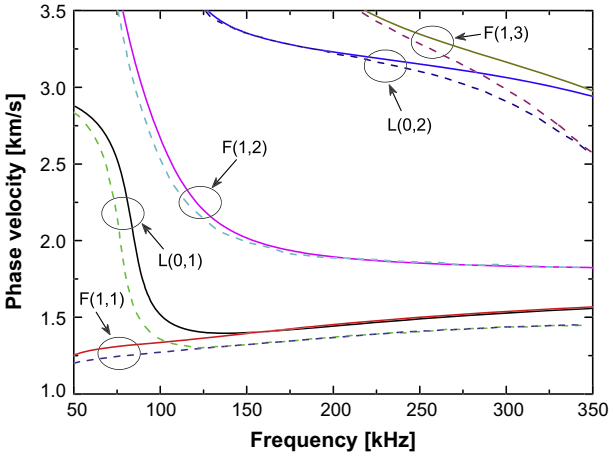

Fig. 2. Dispersion curve of cylindrical Lamb waves in (a) a free bone tube (solid lines) and (b) a bone tube covered with a layer of fluid (thickness:1 mm) (dash lines).

Table 1
Material properties of human cortical bone and composite bone samples.

	Density (kg/m^3)	Young's modulus (GPa)	Poisson's ratio	Bulk modulus (GPa)
Cortical bone	1850	16.46	0.373	
Composite tube	1640	16	0.31	
Fluid	1000			2.2

distinctly from their counterparts in the free bone cylinder. Such a phenomenon was also observed in previous studies [19,26,27,33]. This considerably underpins the concern on the influence arising from soft tissues on the wave propagation in bones. Such an influence may impair the evaluation addressed by QUS techniques, if it is not well considered and appropriately compensated. On the other hand, although it yields valuable information regarding the coupling effect of soft tissues, the theoretical FSB model is significantly simplified for imitating the SBC medium, in that soft tissue is not actually pure fluid, but a kind of soft substance that sustains shear stresses. However, a model dedicated for mimicking the realistic SBC medium is so far unavailable, because both the soft tissue and bone are complex materials, exhibiting strong inhomogeneity and anisotropy, as well as viscoelasticity to a certain degree. With such a concern, cylindrical Sawbones phantoms covered with mimicked soft tissues, and an *in vitro* porcine femur can provide valuable information for understanding the coupling effect of the soft tissue on ultrasound wave propagation.

3. Methodology

3.1. Tubular sample coupled with mimicked soft tissues

A number of composite tubes (Sawbones, Pacific Research Laboratory Inc., Vashon, WA; length: 260 mm, outer radius: 20 mm, thickness: 3 mm) were used to mimic human lone bones, with the recognition of their similarity in morphology and material property, as compared in Table 1. To introduce the effect of coupled soft tissues, a piece of ASR (*soft phase* hereinafter) was manually placed in contact to the outer surface of the composite tube (*hard phase hereinafter*), as listed in Table 2. The ASR is a kind of soft substance that demonstrates highly close properties to those of human soft tissues, regarded as a TEM [6]. The interface between the soft and hard phases was intensively adhered by introducing a specific glue water (Type 460, Boluo Yongqiang Chemical Co., Ltd, China), in recognition of the fact that the soft tissue and bone are compactly connected *in vivo*. Such an adhesive introduces a very thin layer between the soft and hard phases, and was assumed not to influence the competence of the proposed model for evaluating the coupling effect on wave propagation. Before adhering, the contacting surfaces of both phases were cleaned and processed with a finishing agent, to improve adhesion quality in between.

Table 2
Description of synthesised soft tissue–bone phantoms.

Sample No.	Thickness of ASR (mm)	Elastic modulus of ASR (kPa)
0# (no ASR)	0	N.A.
ASR of different thicknesses		
T1#	0.8	11.96
T2#	1.9	*ditto*
T3#	3.4	*ditto*
T4#	4.2	*ditto*
T5#	5.1	*ditto*
T6#	6.3	*ditto*
T7#	7.7	*ditto*
T8#	9.4	*ditto*
ASR of different elastic moduli		
E1#	3.4	2.89
E2#	*ditto*	6.86
E3#	*ditto*	11.96
E4#	*ditto*	19.65
E5#	*ditto*	32.38
E6#	*ditto*	55.87
E7#	*ditto*	73.41
E8#	*ditto*	119.62
E9#	*ditto*	181.23
E10#	*ditto*	336.87
E11#	*ditto*	536.51

The produced ASR samples as described above were of different thicknesses and varied elastic moduli for mimicking soft tissues at various skeletal sites and in different pathological conditions. This was achieved by controlling the shares of silicone gel (Wacker M4600A), firming agent (Wacker M4600B) and oil (AK35, all from Wacker Chemicals (Hong Kong) Ltd.) in the mixture. The detailed manufacturing procedure for producing ASR and mechanical testing for the elastic property of the ASR can be referred to our previous publication [19]. Two series of ASR pieces of the same in-plane dimension (160×60 mm^2) were produced, with one of a fixed elastic modulus (11.96 kPa) but varied thicknesses (from 0.8 to 9.4 mm, Sample No. T1#–T8# in Table 2), and the other of a fixed thickness (3.4 mm) but varied elastic moduli (from 2.89 to 536.51 kPa, Sample No. E1#–E11# in Table 2).

Ultrasonic investigation was performed on the produced SBC phantoms (as listed in Table 2) in terms of the axial transmission measurement in a laboratory setting in the room temperature. All the phantoms were clamped on their two edges on an optical testing table (NEWPORT® ST-UT2). A pair of ultrasound transducers (IS0202HP, Valpey Fisher Corporation®, central frequency: 1 MHz, nominal diameter: 9 mm), with one serving as the wave transmitter and the other as the receiver, were collocated at the interface of the soft and hard phases in tandem. Note that the diameter of transducer is comparable to the wavelength of the wave modes investigated in this study (around 8–15 mm). To obtain good mechanical and acoustical coupling between the ultrasonic transducers and tubular samples, each transducer was placed on an acrylic wedge. One surface of the wedge had the same curvature as that of the tube, as seen in the insert of Fig. 3(a), enabling them to be in close contact with the curved surface of the tube. By that means, the transducer-generated waves could be transmitted efficiently into the samples through the wedge. Both transducers were instrumented with a signal generation and data acquisition system configured on a VXI platform [27], as schematically indicated in Fig. 3(a). The diagnostic signals, i.e., five-cycle Hanning-windowed sinusoidal tonebursts, were generated using an arbitrary waveform generation unit (Agilent® E1441), in which *D*/*A* conversion was performed. The analog signals were amplified to 180 V (peak-to-peak) with a linear amplifier (PiezoSys® EPA-104) to drive the transmitter. Wave signals were captured with the receiver through a signal digitizer (Agilent® E1438A) at a sampling rate of 40 MHz. Shielded wires and standard BNC connectors were used to minimize the noise. Fig. 3(b) displays the photo of experimental setup.

It is noteworthy that, aimed at exploring the coupling effect of mimicked soft tissues on ultrasonic waves in the bone phantoms, the transducer pair was intentionally positioned at the interface of the two media, rather than atop the soft phase, which was different from the actual clinical implementation of QUS. A comparative test (to be detailed in Section 4.1.2) has demonstrated that, when the soft tissue layer is of a small thickness, the velocities of FAS and SAS captured at the interface and those captured atop the soft phase are identical (but not the signal magnitude), because the

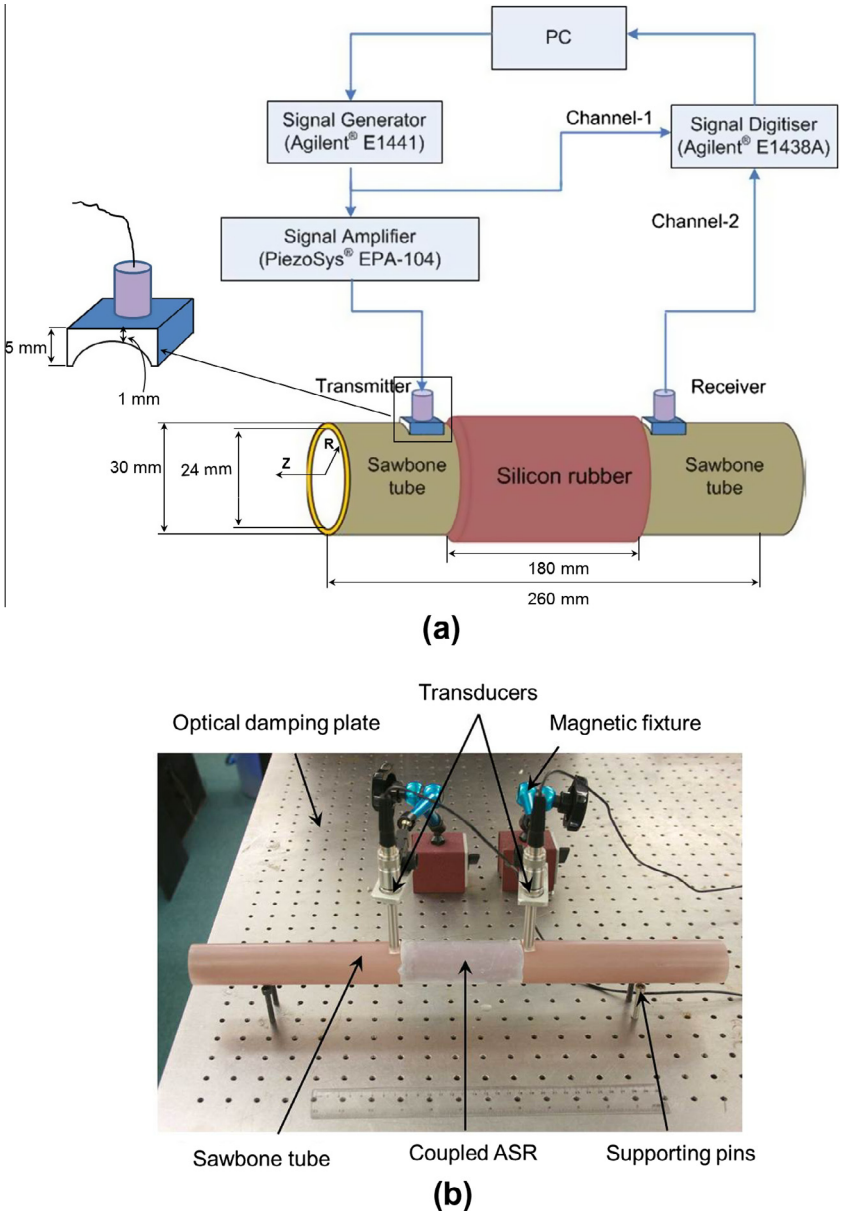

Fig. 3. (a) Illustration and (b) photograph of experimental setup.

time-of-flights used for both wave modes to pass through the thin soft tissue layer are negligible.

3.2. Porcine femur with coupled soft tissues

In addition to the above investigation on SBC phantoms, an *in vitro* porcine femur (bought from the slaughterhouse right after the swine was slaughtered but with soft tissue remained) was tested, as photographed in Fig. 4(a). The marrow of the femur was removed, resulting in an approximately uniform bone thickness being 3 mm along the circumference, as indicated in Fig. 4(b). A test was first carried out on the porcine femur with the transducers positioned on the upper surface of the soft tissue, with the distance between the transmitter and receiver being 82 mm (Fig. 4(a)). The thickness of the soft tissue under test was around 3 mm. Consequently, the soft tissue was removed, as demonstrated in Fig. 4(c), from which it can be noticed that the soft tissue and bone are compactly connected. This is supportable for using adhesive to treat the interface of the SBC phantoms as aforementioned. A second test was then performed by putting the transmitter and receiver on the surface of the bone, as shown in Fig. 4(d), with the distance between the transmitter and receiver kept the same as that in the case shown in Fig. 4(a). In each test, five measurements were taken with the average serving as the final result to reduce errors arising from operations and variations in surrounding environments. The acoustic coupling between the transducers and the bone was guaranteed by introducing a coupling gel (AQUASONIC®, Parker Laboratories, INC., The Netherlands) in between, as indicated in Fig. 4(d). Diagnostic signals as described in Section 3.1.2 were excited at several candidate frequencies swept from 150 kHz to 250 kHz at an increment of 25 kHz.

3.3. Signal processing method

In QUS practice, captured ultrasound signals are prone to a diversity of contaminations including random electrical/magnetic interferences, mechanical noise, temperature/humidity fluctuation and measurement uncertainties. Toward this, a series of signal

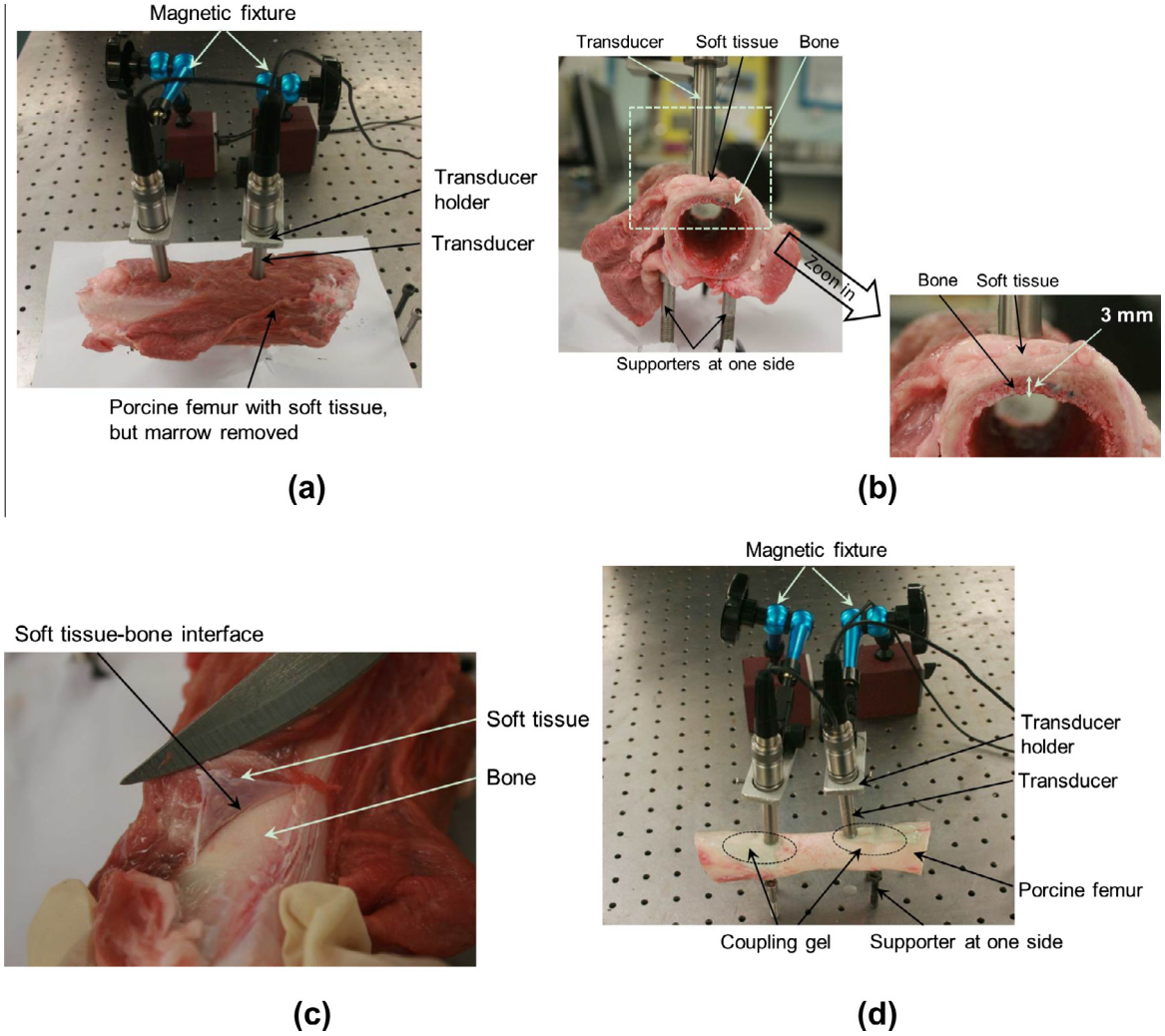

Fig. 4. Photograph of experimental setup for *in vitro* testing using porcine femur coupled with soft tissues: (a) overview and (b) side view; (c) the soft tissue–bone interface; and (d) experimental setup of porcine femur without soft tissue.

processing endeavors, including standard signal pre-processing (signal averaging, DC offset, smoothing and de-noising) and wavelet transform-based signal decomposition was applied, to decompose an acquired signal into different frequency bands, and only the wave components in the excitation frequency band were focused on after screening broadband noise. Considering that wave propagation in an elastic medium is the continuous transportation of energy, distribution of signal energy were obtained using Hilbert-transform (HT). The theorem of HT is described by [34]

$$H(t) = \frac{1}{\pi}\int_{-\infty}^{+\infty}\frac{f(\tau)}{t-\tau}d\tau, \tag{7}$$

where $H(t)$ is the HT of signal $f(t)$. Eq. (7) performs a 90° phase-shift or quadrature filter to construct a so-called analytic signal $F_A(t)$:

$$F_A(t) = f(t) + iH(t) = e(t)\cdot e^{i\phi(t)}, \tag{8a}$$

$$e(t) = \sqrt{f^2(t)+H^2(t)}, \text{ and } \phi(t) = \frac{1}{2\pi}\cdot\frac{d}{dt}\arctan\frac{H(t)}{f(t)}, \tag{8b}$$

whose real part is signal $f(t)$ itself and imaginary part is its corresponding HT, i.e., $H(t)$. $e(t)$ is the module of $F_A(t)$ and $\phi(t)$ is the instantaneous frequency of $F_A(t)$. The envelope of $e(t)$ depicts the energy distribution of $f(t)$ in the time domain. With the operation of HT, the captured signals can be transferred to their counterparts of energy distribution in the same time range, where individual wave components of the signal can be recognized clearly, to be demonstrated in next session.

4. Results and discussion

4.1. Soft tissue–bone-coupled phantom

4.1.1. Mode identification

The experimentally obtained group velocities of FAS and SAS in the free composite tube (Sample No. 0#) were compared with the theoretically calculated dispersion curves of $L(0, 2)$ and $F(1, 1)$ in the structure of same geometrical and material properties with those of Sample No. 0#, for exploring the mode natures of FAS and SAS. Note that the theoretical dispersion curves were obtained using the software package *DISPERSE*®. As demonstrated in Fig. 5, it can be seen that the experimentally obtained dispersion curves of FAS and SAS well fit those of $L(0, 2)$ and $F(1, 1)$, respectively, articulating that FAS is in conformity to $L(0, 1)$, while SAS is in conformity to $F(1, 1)$. Such a conclusion is also consistent with those of previous studies [11,23]. In addition, $L(0, 2)$ is equivalent to the lowest-order symmetric Lamb mode (i.e., S_0) in plate/shell-like structures in terms of particulate vibration, because both of them possess a dominant in-plane vibration of particle [11]. Similarly,

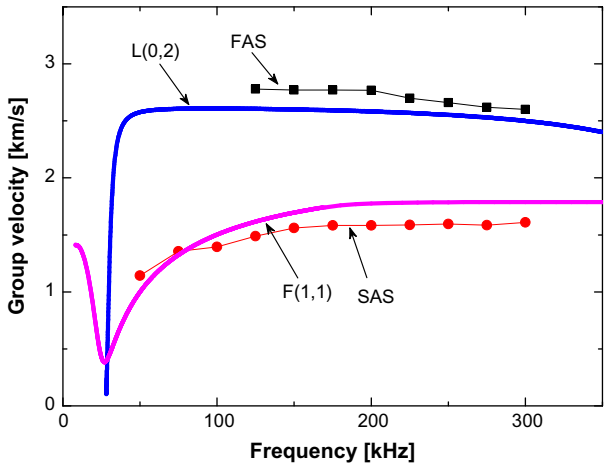

Fig. 5. Numerically and experimentally obtained dispersion curves of guided waves in the composite tube (Sample No. 0#).

SAS is equivalent to the lowest-order anti-symmetric Lamb mode (i.e., A_0) in plate/shell-like structures, as they have a same dominance of out-of-plane particle vibration [23]. Both wave modes can be identified based on their velocities compared with the theoretical values.

4.1.2. Coupling effect on FAS and SAS

4.1.2.1. Different measurement configurations. As addressed in Section 3.1.2, the transducer pair was purposely positioned at the interface of two phases, rather than atop the soft phase (the clinical practice), with a purpose of exploring the coupling effect of soft phase on wave propagation in the hard phase. To examine the difference between these two measurement configurations, a comparative test was carried out, in which FAS and SAS were captured when (i) both transducers were collocated at the interface of two phases as shown schematically in Fig. 6(a) and (ii) both transducers were placed atop the soft phase (Fig. 6(b)). The same ASR layer (elastic modulus: 11.96 kPa; thickness: 3.4 mm) was used in both configurations, and the distance between the transmitter and receiver was kept the same (132 mm).

The HT-processed signals captured under the two configurations are compared in Fig. 7(a). It can be seen that, for either FAS or SAS, the arrival time remains the same (no change in propagation velocity) no matter it is captured at the interface or atop the soft phase; whereas magnitudes of the peak energy of both modes are much attenuated if signals captured atop the soft phase. Conclusion can therefore be drawn that the discrepancy in the propagation velocities of FAS and SAS, when acquired at the interface or atop the soft tissue, is ignorable, provided that the dimension in thickness of the soft tissue is much smaller than the axial dimension of the bone between the transmitter and receiver, i.e., the distance between the transmitter and receiver in the axial transmission measurement (the case in the current study). In this sense, all the calibrated coupling effect of the soft tissue on FAS and SAS, obtained in the above using transducers collocated at the interface of two phases, is comparable with that in real clinical setting where the transducers are placed atop human soft tissues.

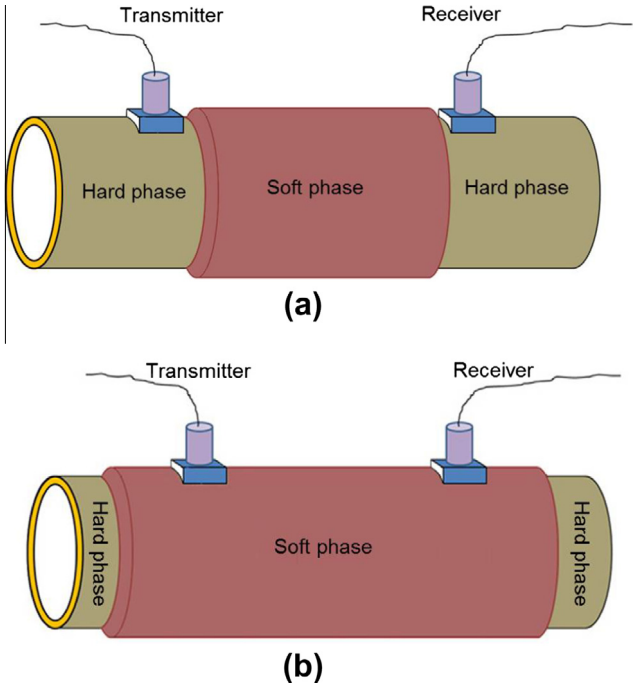

Fig. 6. Schematic illustrations of two different measurement configurations with the transmitter and receiver placed (a) at the interface of soft and hard phases and (b) atop the soft phase.

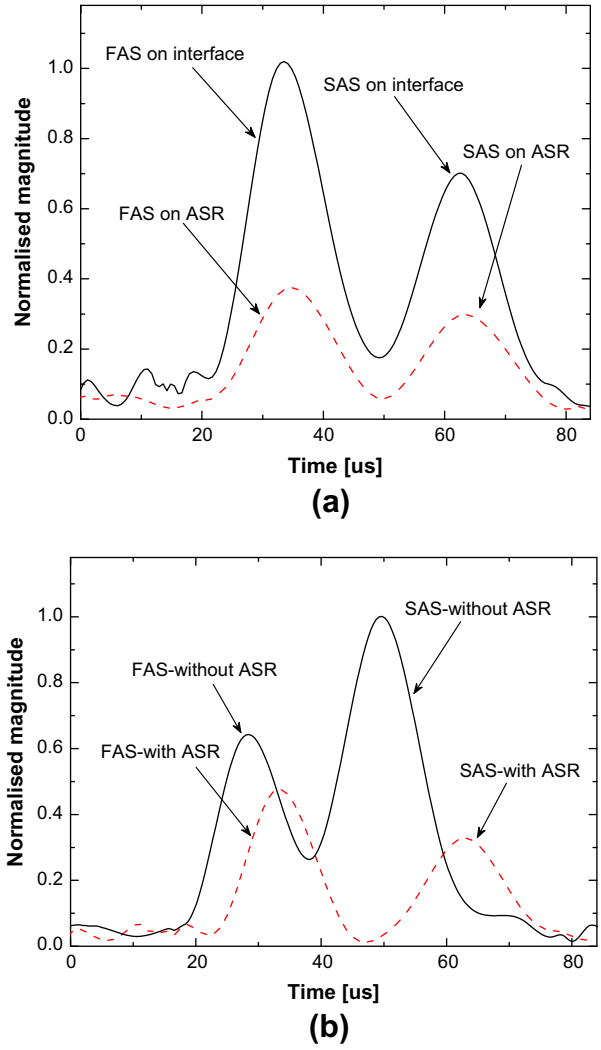

Fig. 7. (a) Comparison of HT-processed results of signals captured under two different measurement configurations as illustrated in Fig. 6 and (b) HT-processed signals captured from Sawbones tube in the absence and presence of a layer of ASR (thickness of ASR layer: 3.4 mm).

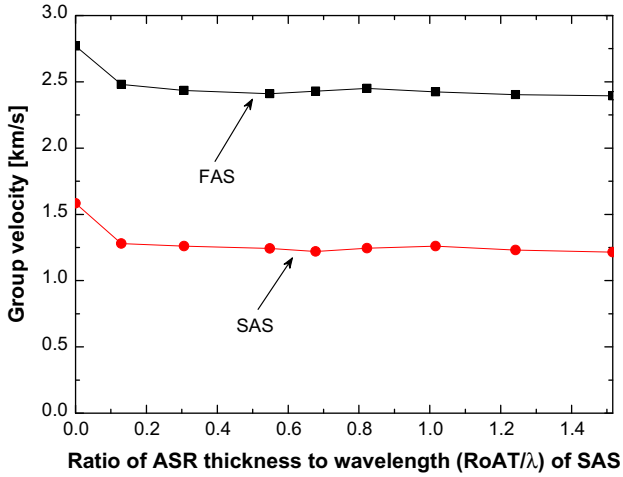

Fig. 8. Group velocities of FAS and SAS in bone phantoms (Sample No. 0#, T1#–T8#) vs. RoAT/λ of SAS.

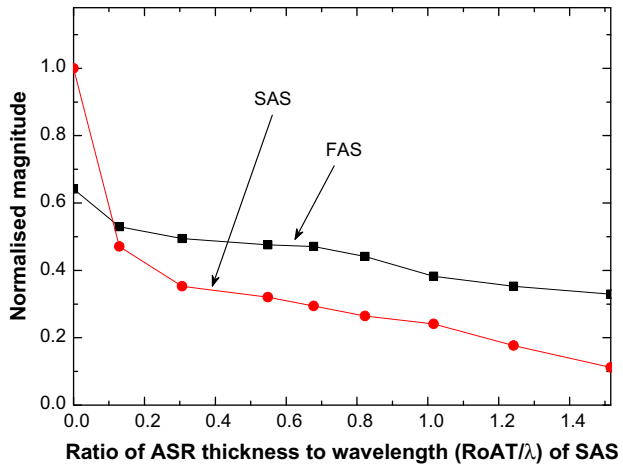

Fig. 9. Magnitudes of FAS and SAS in bone phantoms (Sample No. 0#, T1#–T8#) vs. RoAT/λ of SAS (signal magnitude being normalized relative to the amplitude extremum of the signal in Sample No. 0#).

4.1.2.2. Effect of thickness and elastic modulus of mimicked soft tissues. As a representative example, Fig. 7(b) displays the HT-processed signals captured from the composite tube in the absence (Sample No. 0#) and presence (Sample No. T3#) of ASR at frequency of 200 kHz, to find that the presence of a layer of ASR causes significant changes to both FAS and SAS. Such a modulation is twofold: (i) the arriving time of both wave modes in the phantom coupled with soft phase delayed comparing with their counterparts in the free phantom (without soft phase), inferring that FAS and SAS have reduced propagation velocities in the presence of soft phase and (ii) magnitudes of both modes decrease to a prominent extent, possibly due to the fact that a layer of ASR provides a way for the wave energies to leak from the hard phase to the soft phase, which consumes a certain portion of the energies of both wave modes before their arrival at the receiver.

To further explore the coupling effect of soft phase on the two modes, measurements were conducted on a series of soft tissue–bone mimicking phantoms (as described in Section 3.1.1) with the soft phase varying in thickness (Sample No. T1#–T8#, Table 2) and elastic modulus (Sample No. E1#–T11#, Table 2) at the frequency of 200 kHz. Such a design is deliberately to imitate the biological conditions of soft tissues at different skeletal sites from the health to the diseased. Fig. 8 shows the relationship of velocities of FAS and SAS and ratio of ASR thickness to the wavelength (RoAT/λ) of SAS, to find that the velocities of both modes reduced to a great deal no sooner than the soft phase was introduced, but future variation in RoAT/λ does not introduce much change to the velocities of both FAS and SAS. It is inferred that the coupling effect on velocities of both modes may be regionally limited, i.e., the coupling effect may take place in a limited thickness of soft tissue. Furthermore, as can be learn from the figure, the presence of soft phase causes an approximately constant reduction in velocity of around 10% for FAS and circa 20% for SAS at different RoAT/λ, indicating that the modulation on wave velocity due to the presence of soft tissue can be compensated for regardless of RoAT/λ. On the other hand, as manifested in Fig. 9, alien from the velocity, the magnitudes of both modes demonstrated a continuous decrease as RoAT/λ increases, articulating that such a coupling effect consistently exists with respect to signal magnitude. The reduction rates in signal magnitudes of both FAS and SAS in the free phantom (without soft phase) with respect to the values in the phantom with soft phase are indicated to increase as RoAT/λ increases, possibly due to the increase in wave propagation path within the soft

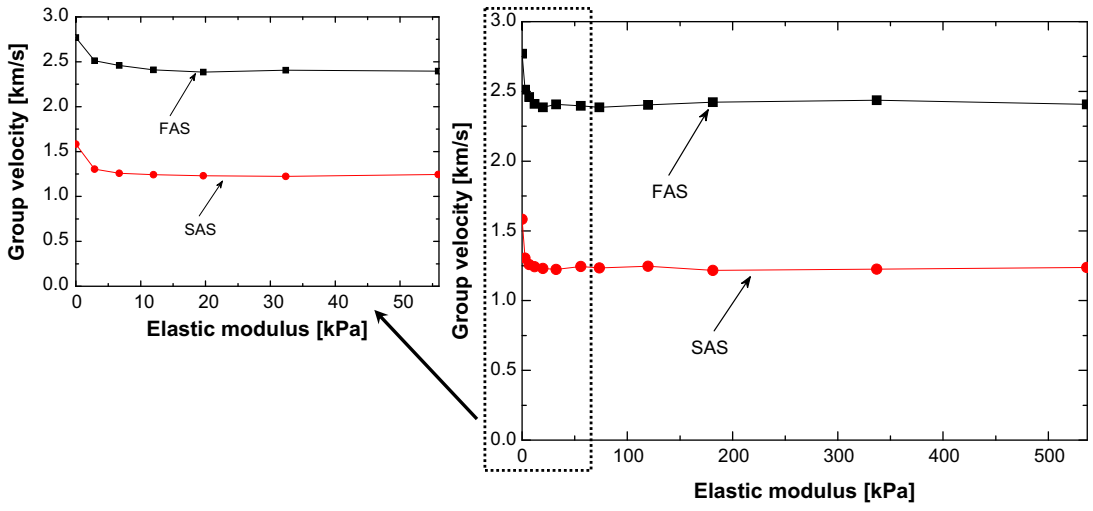

Fig. 10. Group velocities of FAS and SAS in bone phantoms (Sample No. 0#, E1#–E11#) vs. elastic modulus of coupled ASR layer (insert: zoomed-in part showing initial stage).

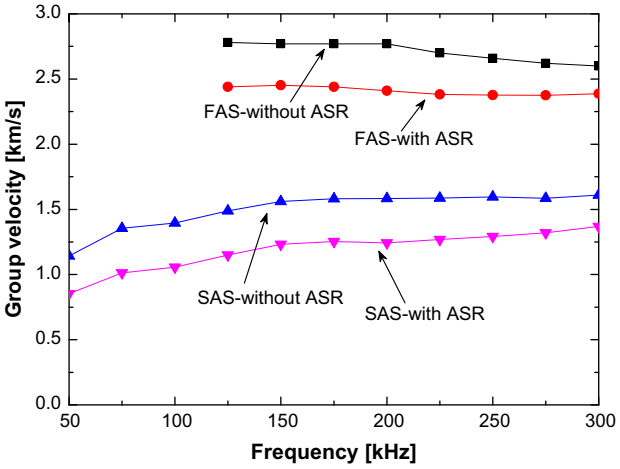

Fig. 11. Dispersion curves for FAS and SAS in bone phantoms without (Sample No. 0#) and with a coupled ASR layer (3.4 mm thick as an example, Sample No. T3#).

phase as RoAT/λ increases. The observations are similar with those from our previous publication [19].

Further, as noticed from Figs. 8 and 9, the SAS shows a greater reduction in either velocity or magnitude due to the presence of soft phase than FAS, highlighting that SAS has a greater sensitivity to the coupling effect. This may be contributed to (i) the shorter wavelength of SAS than FAS, which makes SAS have higher sensitivity to the coupling effect and (ii) the different particulate vibration manners of FAS and SAS at the soft–hard interface: FAS is equivalent to $L(0, 1)$ which has a predominant in-plane particulate vibration, while SAS, being equivalent to $F(1, 1)$ has particle vibrating most in the out-of-plane direction. It is the out-of-plane vibration mode that causes the energy of SAS more easily to pass across the soft–hard interface from the hard phase to the soft phase than that of FAS, leading to significant energy consumption and making SAS more affected by the coupling effect. (Note that $F(1, 2)$ was not detected possibly because $F(1, 2)$ is a high-order mode and cannot be generated easily and (ii) this mode is highly attenuated in the samples.) However, the high sensitivity of SAS to the coupling effect may undermine its prevalence and capacity in bone evaluation, although SAS has been reported to be a prominent indicator to osteoporosis development [29]. It thus entails the current study to explore such an effect and develop a method to compensate for it. Note that as SAS has a higher sensitivity to the coupling effect, the thickness of the ASR layer was intentionally normalized with respective to the wavelength of SAS, as indicated in Figs. 8 and 9.

Fig. 10 demonstrates the relationships of group velocity vs. variation in elastic modulus of the coupled soft phase. Similar to the thickness scenario, the influence of soft phase takes effect most in the moment when the soft phase was introduced; further increase in elastic modulus does not change the velocity of FAS and SAS prominently. As can be calculated from Fig. 10, the reduction in propagation velocity is either circa 20% for SAS or around 10% for FAS, and such a reduction for SAS or FAS remain approximately at different elastic moduli. This may make it possible to compensate for the coupling effect on wave velocity arising from the soft tissue regardless of the tissue elastic property. Furthermore, the reduction in propagation velocity shows a higher value for SAS than for FAS, confirming that SAS has a higher sensitivity to the coupling effect than FAS.

4.1.2.3. Dispersion properties of FAS and SAS. Extending to a wide frequency range, the above investigation was iterated on Samples No. 0# and No. T3# by swapping the excitation frequency from

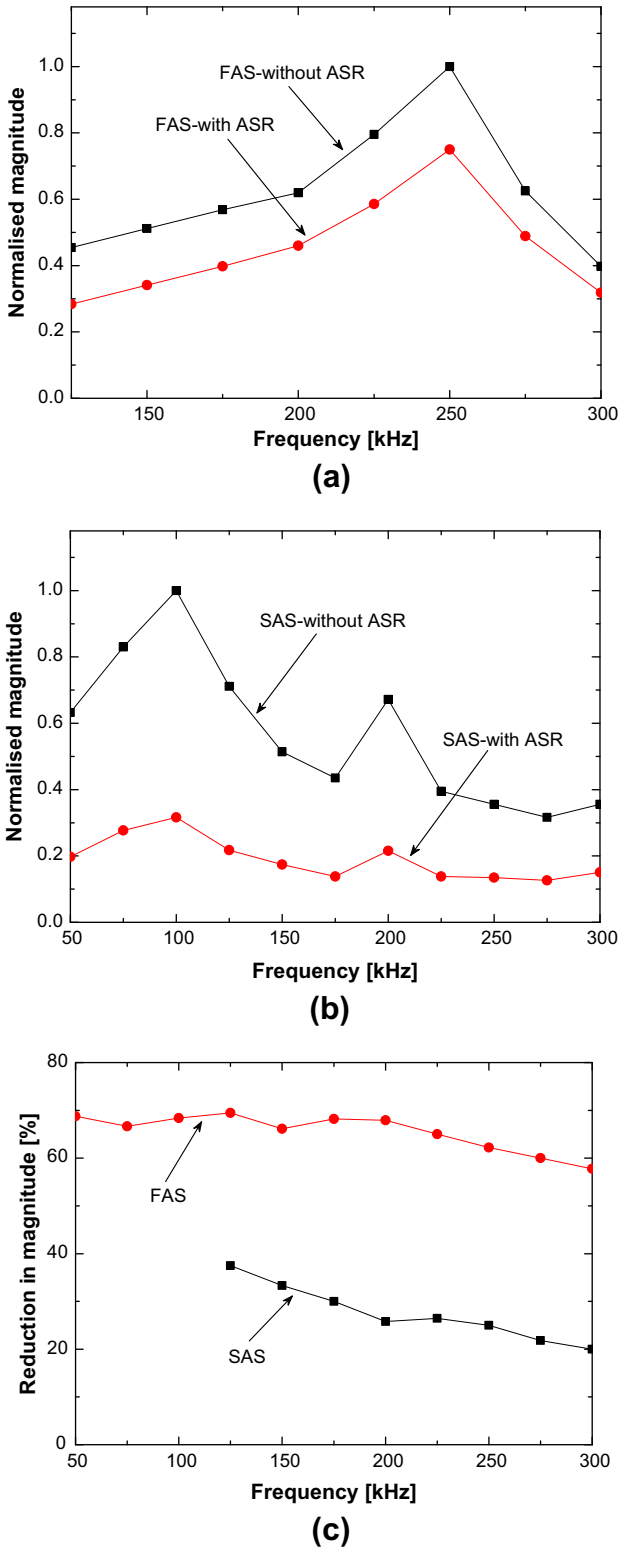

Fig. 12. Magnitude of (a) FAS and (b) SAS in the absence and presence of ASR at different frequencies; (c) reductions in magnitude of FAS and SAS due to coupling ASR at different frequencies.

50 kHz to 300 kHz with an increment of 25 kHz. The captured group velocities of FAS and SAS are shown in Fig. 11, to observe that the velocity of either FAS or SAS reduces to a prominent degree due to the presence of a layer of ASR at every examined excitation frequency. Note that FAS is undetectable at frequencies

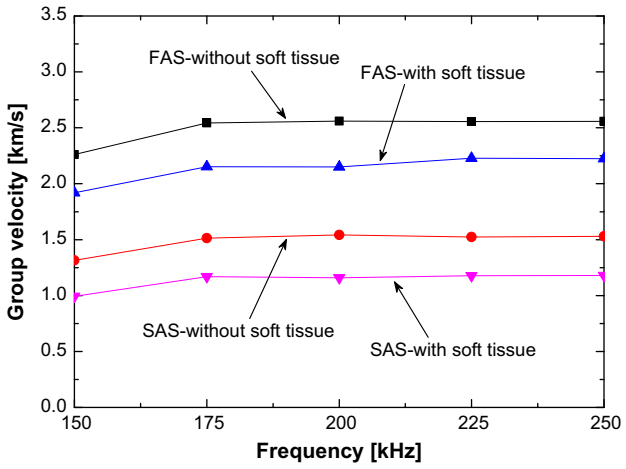

Fig. 13. Dispersion curves for FAS and SAS in porcine femur with and without soft tissue.

below 125 kHz. It is also indicated that SAS presents greater reduction in velocity than FAS at each frequency, corroborating the previous statement that SAS has a higher sensitivity to the coupling effect than FAS.

In addition to the investigation on the wave velocity, Figs. 12(a) and 12(b) show the magnitudes of FAS and SAS, respectively, captured in bone phantoms without and with a layer of ASR in the frequency range of 125–300 kHz for FAS and 50–300 kHz for SAS. The coupling effect of soft phase on the FAS and SAS can be intuitively observed from the plot, in which the magnitudes of the both modes reduced significantly at every frequency due to the presence of soft phase. It can be also noticed that both FAS and SAS have their respective magnitude dominance in the discussed frequency range, e.g., the amplitude of SAS hits its peak at the frequency of 200 kHz, which is right the frequency of the diagnosis signal in this study (Section 4.1.2.1). On the other hand, though the ASR layer caused significant reduction in signal magnitude at each frequency, it does not alter the magnitude dominance of either FAS or SAS. This can be instructive in mode selection especially for the QUS for bone assessment where the soft tissue attenuates the wave energy at a great level. Fig. 12(c) presents the reduction in magnitudes of FAS and SAS due to the presence of soft phase in the above mentioned frequency range, to find that SAS demonstrates a greater reduction in magnitude than FAS as a result of the coupling effect arising from soft phase. Such an observation is similar with that from Figs. 8 and 9, possibly due to the same reason in terms of the difference in the particulate vibration patterns of FAS and SAS as above analyzed.

4.2. Porcine femur

Further, the coupling effect of soft tissue on wave propagation was explored on a porcine femur with marrow removed by testing two distinct scenarios: (i) with the soft tissue (Fig. 4(a)) and (ii) without soft tissue (Fig. 4(d)). Fig. 13 plots the group velocities of FAS and SAS captured in those two scenarios at frequencies from 150 to 250 kHz with an increment of 25 kHz. Although they were confined to a limited range due to the practical limitation, the examined frequencies guaranteed that the capture signal can be well recognized and has a good signal-to-noise ratio. In addition, the frequency range covered the most commonly used diagnosis frequencies in practice [23,29,35]. The data in Fig. 13 highlights that the ultrasonic waves, including FAS and SAS, behave fairly distinctly in the bone with soft tissue from their counterparts in the bone without soft tissue, manifested as significant reductions in

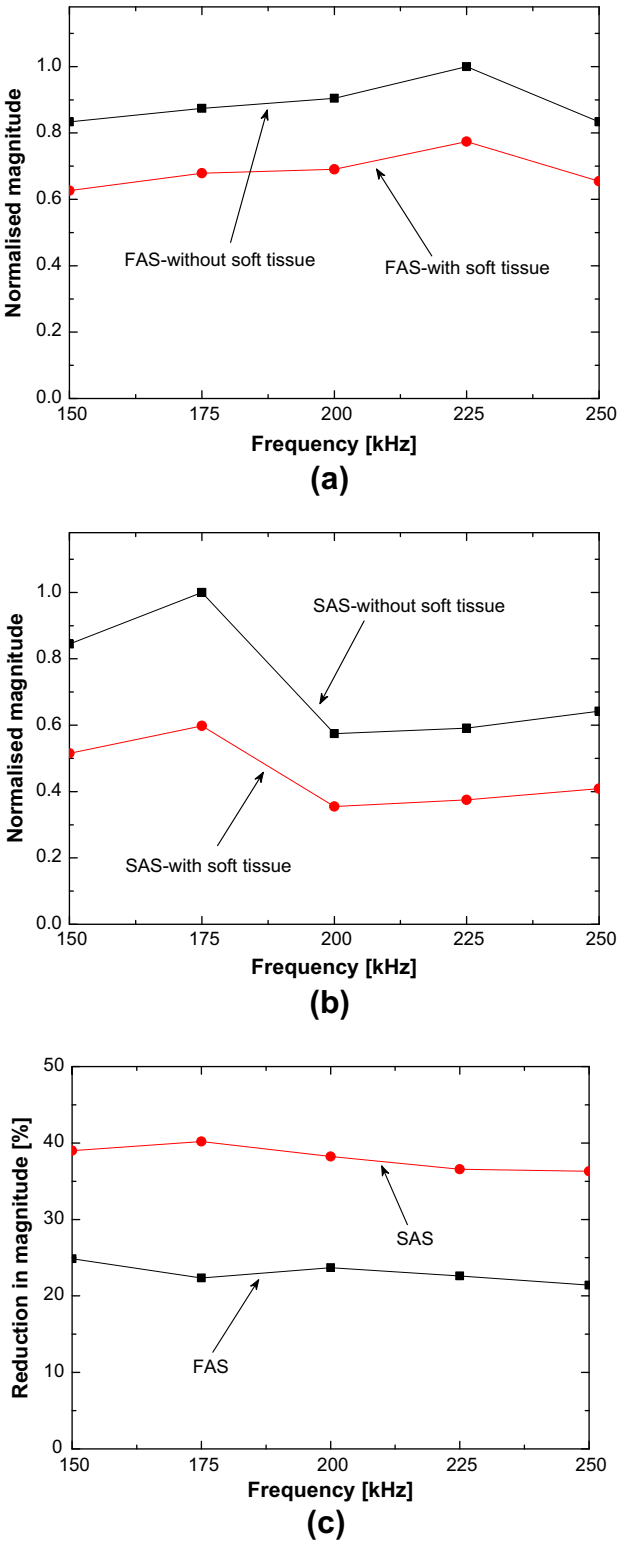

Fig. 14. Magnitude of (a) FAS and (b) SAS in porcine femur with and without soft tissue at different frequencies; and (c) reductions in magnitude of FAS and SAS in porcine femur with at different frequencies.

velocity of each mode at every examined frequency. Such a distinction is fully attributed to the presence of soft tissue, which is consistent with observation from the phantom studies (Section 4.1.2.3). Noted that the contribution from the thickness of the soft tissue was ignored here, as the measurement points were

selected to have a thin soft tissue layer (circa 3 mm). As investigated in Section 4.1.2.1, there is no much difference in velocity of FAS or SAS in the bone with and without soft tissue when the soft tissue layer is of small thickness. As can be learned from Fig. 13, the reduction rates in velocities of both modes due to the presence of the soft tissue does not change much in the examined frequency range, although it demonstrates a slight trend of decreasing. It infers that the soft tissue poses an approximate constant coupling effect on the wave propagation in the bone within the examined frequency range, potentially paving the way for compensation for such an effect regardless of the excitation frequency, toward high precision bone evaluation. Furthermore, the reduction in velocity of SAS due to the presence of the soft tissue (around 25%) demonstrates higher value than that of FAS (circa 15%), indicating that SAS is more sensitive to the coupling effect of the soft tissue, which corroborates the previous conclusion from the phantom studies (Section 4.1.2).

In parallel to the above interrogation on wave velocity, signal magnitudes of both FAS and SAS were also canvassed, as displayed in Fig. 14(a) for FAS and Fig. 14(b) for SAS. Similar observations can be obtained to those from the phantom study (Section 4.1.2):

(i) the FAS and SAS exhibit distinct magnitude dominances from each other, e.g., FAS has its maximum in magnitude at the frequency of 225 kHz, while SAS at 175 kHz, which are slightly lower than their counterparts in the phantom study, respectively. Such a small distinction for either FAS or SAS may be contributed to the difference in material properties of the porcine femur and those of composite tubes; and
(ii) the presence of a layer of soft tissue does not alter the variation trend of the signal magnitude in the examined frequency domain. This is consistent with the observation from the phantoms studies as stated in Section 4.1.2.3.

Fig. 14(c) plots the reduction rates in magnitudes of FAS and SAS in the porcine femur with soft tissue comparing with those without soft tissue, to find that in the examined frequency domain (i) the soft tissue causes a nearly uniform impact on the magnitude of either FAS or SAS; and (ii) such an impact in signal magnitude is more prominent for SAS (around 40%) than for FAS (circa 25%), corroborating the conclusion that SAS is more sensitive to the coupling effect of soft tissue than FAS.

5. Conclusions

In clinic, human soft tissues may impair the precision and accuracy of QUS assessment for human bones. In this study, the coupling effect of the soft tissue was systematically investigated via ultrasonically interrogating a series of soft tissue–bone-coupled phantoms by varying the thickness and elastic modulus of the ASR layers, as well as an *in vitro* porcine femur. The results convinced that (i) the coupling effect arising from soft tissues significantly affects the propagation characteristics of ultrasonic waves in the bone, manifesting as reduced propagation velocities and attenuated signal magnitudes; (ii) such an effect is not dependent on the variations in thickness and elastic modulus of the soft tissue; and (iii) SAS has a higher sensitivity to the coupling effect from soft tissue than FAS. It is concluded that the coupling effect of soft tissue calls for careful consideration, especially when using SAS, and can be quantitatively compensated for regardless of the properties of the soft tissue layer (the coupling effect caused reduction in velocity is 15% for FAS or 25% for SAS, based which the coupling effect can be compensated). This study contributes to an effort of driving QUS toward a bone evaluation technique of high precision and accuracy.

Acknowledgement

The work was supported by a grant from the Hong Kong Polytechnic University (Project No.: G-UA80).

References

[1] P. Laugier, G. Haïat, Bone Quantitative Ultrasound, Springer, New York, 2011.
[2] M. Grigoryan, J.A. Lynch, A.L. Fierlinger, A. Guermazi, B. Fan, D.B. MacLean, A. MacLean, H.K. Genant, Quantitative and qualitative assessment of closed fracture healing using computed tomography and conventional radiography, Acad. Radiol. 10 (2003) 1267–1273.
[3] Y. Wang, D.B. Plewes, An MRI calorimetry technique to measure tissue ultrasound absorption, Magn. Reson. Med. 42 (1999) 158–166.
[4] S.H. Prins, H.L. Jørgensen, L.V. Jørgensen, C. Hassager, The role of quantitative ultrasound in the assessment of bone: a review, Clin. Physiol. 18 (1998) 3–17.
[5] C.F. Njeh, C.M. Boivin, C.M. Langton, The role of ultrasound in the assessment of osteoporosis: a review, Osteoporosis Int. 7 (1997) 7–22.
[6] C.F. Njeh, J.R. Kearton, D. Hans, C.M. Boivin, The use of quantitative ultrasound to monitor fracture healing: a feasibility study using phantoms, Med. Eng. Phys. 20 (1999) 781–786.
[7] C. Roux, V. Roberjot, R. Porcher, S. Kolta, M. Dougados, P. Laugier, Ultrasonic backscatter and transmission parameters at the os calcis in postmenopausal osteoporosis, J. Bone. Miner. Res. 16 (2001) 1353–1362.
[8] A. Tatarinov, N. Sarvazyan, A. Sarvazyan, Use of multiple acoustic wave modes for assessment of long bones: model study, Ultrasonics 43 (2005) 672–680.
[9] D.A. Ta, K. Huang, W.Q. Wang, Y.Y. Wang, L.H. Le, Identification and analysis of multimode guided waves in tibia cortical bone, Ultrasonics 44 (2006) e279–e284.
[10] A. Sarvazyan, A. Tatarinov, V. Egorov, S. Airapetian, V. Kurtenok, C.J. Gatt Jr., Application of the dual-frequency ultrasonometer for osteoporosis detection, Ultrasonics 49 (2009) 331–337.
[11] M.J.S. Lowe, D.N. Alleyne, P. Cawley, Defect detection in pipes using guided waves, Ultrasonics 36 (1998) 147–154.
[12] M.E.-C. El-Kettani, F. Lupp, A. Guillet, Guided waves in a plate with linearly varying thickness: experimental and numerical results, Ultrasonics 42 (2004) 807–812.
[13] M. Muller, P. Moilanen, E. Bossy, P. Nicholson, V. Kilappa, J. Timonen, M. Talmant, S. Cheng, P. Laugier, Comparison of three ultrasonic axial transmission methods for bone assessment, Ultrasound Med. Biol. 31 (2005) 633–642.
[14] V.C. Protopappas, I.C. Kourtis, L.C. Kourtis, K.N. Malizos, C.V. Massalas, D.I. Fotiadis, Three-dimensional finite element modeling of guided ultrasound wave propagation in intact and healing long bones, J. Acoust. Soc. Am. 121 (2007) 3907–3921.
[15] J.-G. Minonzio, M. Talmant, P. Laugier, Measurement of guided mode wave vectors by analysis of the transfer matrix obtained with multi-emitters and multi-receivers in contact, J. Phys.: Conf. Ser. (2011) 012003.
[16] P. Moilanen, Ultrasonic Guided Wave Measurements in Bone, University of Jyväskylä, Jyväskylä, Finland, 2004.
[17] E. Bossy, M. Talmant, M. Defontaine, F. Patat, P. Laugier, Bidirectional axial transmission can improve accuracy and precision of ultrasonic velocity measurement in cortical bone: a validation on test materials, IEEE Trans. Ultrason. Ferroelectr. Freq. Control 51 (2004) 71–79.
[18] P. Moilanen, P.H.F. Nicholson, T. Kärkkäinen, Q. Wang, J. Timonen, S. Cheng, Assessment of the tibia using ultrasonic guided waves in pubertal girls, Osteoporosis. Int. 14 (2003) 1020–1027.
[19] J. Chen, L. Cheng, Z. Su, L. Qin, Modeling elastic waves in coupled media: estimate of soft tissue influence and application to quantitative ultrasound, Ultrasonics 53 (2013) 350–362.
[20] J. Chen, J. Foiret, J.-G. Minonzio, M. Talmant, Z. Su, L. Cheng, P. Laugier, Measurement of guided mode wavenumbers in soft tissue–bone mimicking phantoms using ultrasonic axial transmission, Phys. Med. Biol. 57 (2012) 3025–3037.
[21] J. Chen, Z. Su, L. Cheng, L. Qin, Influence of soft tissues on ultrasonic Lamb waves in synthesised soft tissue–bone phantoms, IFMBE Proc. 31 (2010) 1315–1318.
[22] M.K.H. Malo, J.P. Karjalainen, H. Isaksson, O. Riekkinen, J.S. Jurvelin, J. Töyräs, Numerical analysis of uncertainties in dual frequency bone ultrasound technique, Ultrasound Med. Biol. 36 (2010) 288–294.
[23] P. Moilanen, M. Talmant, V. Kilappa, P. Nicholson, S.L. Cheng, J. Timonen, P. Laugier, Modeling the impact of soft tissue on axial transmission measurements of ultrasonic guided waves in human radius, J. Acoust. Soc. Am. 124 (2008) 2364–2373.
[24] M. Talmant, S. Kolta, C. Roux, D. Haguenauer, I. Vedel, B. Cassou, E. Bossy, P. Laugier, In vivo performance evaluation of bi-directional ultrasonic axial transmission for cortical bone assessment, Ultrasound Med. Biol. 35 (2009) 912–919.

[25] M.G. Vavva, V.C. Protopappas, L.N. Gergidis, A. Charalambopoulos, D.I. Fotiadis, D. Polyzos, The effect of boundary conditions on guided wave propagation in two-dimensional models of healing bone, Ultrasonics 48 (2008) 598–606.
[26] P. Moilanen, P.H.F. Nicholson, V. Kilappa, S. Cheng, J. Timonen, Measuring guided waves in long bones: modeling and experiments in free and immersed plates, Ultrasound Med. Biol. 32 (2006) 709–719.
[27] J. Chen, Z. Su, L. Cheng, Identification of corrosion damage in submerged structures using fundamental anti-symmetric Lamb waves, Smart Mater. Struct. 19 (2010) 015004.
[28] J. Chen, Z. Su, L. Cheng, The medium coupling effect on propagation of guided waves in engineering structures and human bone phantoms, coupled systems mechanics, Int. J. 1 (2013) 297–309.
[29] K.I. Lee, S.W. Yoon, Feasibility of bone assessment with leaky Lamb waves in bone phantoms and a bovine tibia, J. Acoust. Soc. Am. 115 (2004) 3210–3217.
[30] D.C. Gazis, Three-dimensional investigation of the propagation of waves in hollow circular cylinders. I. Analytical foundation, J. Acoust. Soc. Am. 31 (1959) 568–573.
[31] J.D. Achenbach, Wave Propagation in Elastic Solids, North-Holland, Amsterdam, 1973.
[32] C.L. Yapura, V.K. Kinra, Guided waves in a fluid–solid bilayer, Wave Motion 21 (1995) 35–46.
[33] J.D.N. Cheeke, X. Li, Z. Wang, Observation of flexural Lamb waves (A_0 mode) on water-filled cylindrical shells, J. Acoust. Soc. Am. 104 (1998) 3678–3680.
[34] W.J. Staszewski, C. Boller, G.R. Tomlinson, Health Monitoring of Aerospace Structures: Smart Sensor Technologies and Signal Processing, John Wiley & Sons, Inc., New York, 2004.
[35] S.P. Dodd, J.L. Cunningham, A.W. Miles, S. Gheduzzi, V.F. Humphrey, Ultrasound transmission loss across transverse and oblique bone fractures: an in vitro study, Ultrasound Med. Biol. 34 (2008) 454–462.